Colloid Polym Sci (2007) 285:1213–1227
DOI 10.1007/s00396-007-1674-0

ORIGINAL CONTRIBUTION

Studies of optical and structural properties of CdSe/polymer nanocomposites: evidence of charge transfer and photostability

Himani Sharma · Shailesh N. Sharma · Gurmeet Singh · Sonnada Math Shivaprasad

Received: 28 December 2006 / Accepted: 15 March 2007 / Published online: 31 May 2007

Abstract In this work, the role of conducting [poly (p-phenylinevinylene) (PPV)] and nonconducting (polystyrene) polymers on the properties of their respective composites with CdSe quantum dots of varied sizes has been investigated. The emission and structural properties of polymer–CdSe composites are found to be dependent on the crystallite size and morphology of CdSe nanocrystallites. Smaller CdSe quantum dots (size, ~5 nm) ensures efficient charge transfer process across polymer–CdSe interface as evident by almost complete quenching of photoluminescence (PL) emission as compared to larger CdSe quantum dots (size, ~7 nm). Presence of residual trioctylphosphine (TOP)/ tri-*n*-octylphosphine-oxide (TOPO) species and agglomeration of particles act as a hindrance for quenching of emission and hence charge transfer for larger CdSe nanocrystallites. Emission studies indicated an increased conjugation length for PPV polymers in different solvents (toluene, pyridine) and in solid state. Nonconducting polymer polystyrene shows charge transfer across polymer–CdSe interface as well. However, polystyrene polymer has a shorter chain length, which ensures maximum coverage on the surface of CdSe nanocrystallites and provides better photostability to CdSe QDs within the polymer matrix as compared to that for PPV–CdSe nanocomposites.

Keywords CdSe/polymer nanocomposites · PPV · Polystyrene · Optical properties · Structural properties · Charge transfer · Photostability

H. Sharma · S. N. Sharma (✉) · S. M. Shivaprasad
Electronic Materials Division, National Physical Laboratory,
Dr. K. S. Krishnan Marg,
New Delhi 110 012, India
e-mail: shailesh@mail.nplindia.ernet.in

H. Sharma · G. Singh
Department of Chemistry, University of Delhi,
Delhi 110 007, India

Introduction

II–VI nanocrystals (CdS, CdTe, and CdSe) are receiving considerable attention for fundamental studies of zero-dimensional quantum confinement and their color tunability as a function of size for their utilization in a range of applications that includes luminescent devices, biological markers, lasers, and catalysis [1–4]. For this reason, the control and improvement of the luminescence properties of quantum dots QDs has been a major goal in synthetic nanochemistry and related preparative procedures [5, 6].

Colloidal methods provide effective routes to preparing semiconductor nanocrystals that are soluble in organic solvents and have a narrow size distribution [7]. Moreover, surface chemistry is an efficient tool not only to organize and immobilize the nanocrystals but also to effectively modify the emission properties [8, 9]. The possibility of performing the manipulation of prepared nanocrystals by properly engineering the surface by means of capping exchange enables the nanocrystals to be placed in almost any chemical environment, being soluble in organic solvent [10]. Recent efforts have been directed towards the fabrication of polymer nanocomposites containing nanometer-sized crystals of inorganic semiconductors because of their potential application as high technology materials [11, 12]. In nanocomposites, organic polymer cannot only stabilize the

nanoparticles in a solid matrix but also effectively combine the peculiar features of organic and inorganic components, such as the mechanical performances of polymers, and the optical and electronic features of QDs, thus resulting in novel properties [13, 14]. The incorporation of semiconductor nanocrystals within a bulk structure has several advantages over nanoparticles in solution. Solid matrices retain their shape, and polymeric materials can be processed or manipulated into thin films and can be stretched and oriented, etc., opening new perspectives to fundamental studies and to a number of original applications [15]. Theory and experiments have shown that the properties of nanostructured materials strongly vary with the size and shape of the particles [16, 17]. Nanocomposite structures have been used to create optically functional materials to enhance the photoconductivity of host polymers by charge and energy transfer to modify their refractive index, etc. [18, 19]. They have new promising applications in many fields such as mechanics, optoelectronics, catalysis, and biology [20, 21]. Due to this interest, much of the recent research has focused on discovering new routes to preparing monodisperse nanocrystals of semiconductor in the condensed phase.

There are reports describing the preparation of inorganic/polymeric composites in which semiconducting nanocrystals confer specific properties to the composites [22, 23]. Various approaches have been employed to prepare nanoparticle/polymer composites. One approach uses polymer films containing ionic functionals, which can ion exchange with the precursor salt solution of the nanoparticles [24]. When the nanoparticles are eventually formed in situ, a direct encapsulation within the polymer films is thus effected. Hilinski et al. [25] have reported a large third-order nonlinearity of CdS nanocrystallites embedded in Nafion films using this method. Incorporation of CdS nanoparticles into polymer-blend membranes of poly(styrene phophonate diethyl ester) (PSP) and cellulose acetate (CA) has also been reported [26, 27]. On the other hand, Yang et al. [28] have reported the synthesis of PbS and ZnS nanocomposites via the microgels of Pb- or Zn-methylacrylate, which were then copolymerized into polystyrene (PS) matrix. Pavel and Mackay [29] have reported an elegant one-pot synthesis of nanoparticle/polymer composite via a reverse micelle method using polymerizable surfactant system. However, all above approaches for the preparation of nanoparticle/polymer composites are quite complicated. The simplest approach involves spin-casting the pre-prepared nanoparticles together with polymer dissolved in a suitable solvent. However, the procedure inevitably introduces capping molecules employed in the pre-prepared nanoparticles into the composites and also requires the selection of a suitable solvent for both the nanoparticles and the chosen polymer matrix [30].

Thus, there are basically two main approaches that has been recognized, one in which the nanocrystals are generated in the presence of polymers and the other one consisting on the dispersion of previously prepared nanocrystals in polymers. This work deals with the latter method in which CdSe nanocrystals of varied sizes prepared by trioctylphosphine (TOP)/ tri-*n*-octylphosphine-oxide (TOPO) method, i.e., by chemical route, are dispersed in conducting [poly (p-phenylinevinylene) (PPV)] and nonconducting (polystyrene) matrices, respectively. The size, stability, optical, and structural properties of the resulting dispersions could be tailored by the composition and concentration of these polymers. The basic aim of this work has been twofold: (1) to successfully demonstrate the use of CdSe nanocrystals as electron acceptors in conducting polymer (PPV) blends for the study of photo-induced charge separation and (2) the use of nonconducting polymer (polystyrene) as a matrix in effectively enhancing the photostability of the CdSe QDs within the polymer matrix.

Experimental

Nearly monodispersive samples of CdSe nanocrystals were synthesized by the TOPO method employed by Murray et al. as modified by Bowen Katari et al. [6, 31]. The materials used were of the purest quality available and used as received. Conducting PPV polymer and nonconducting polystyrene polymers used were commercially available. The nanoparticle sizes were monitored by varying the precursor ratios of CdO and Se [32, 33]. The TOPO surface ligand was removed from the CdSe samples by washing the nanocrystals three times with methanol and then three times by dissolving them in the minimum quantity of pyridine and precipitating them with hexanes. Displacement of the surface ligand with pyridine is expected to remove approximately 90% of the TOPO originally bound to the surfaces and has been shown to increase charge separation efficiency at polymer/CdSe interfaces [31, 34]. The final nanocrystal precipitate was dissolved in toluene or pyridine without drying. Solutions were mixed to obtain the desired weight ratios of nanocrystal to polymer, and then films were obtained by spin coating on indium–tin oxide (ITO) substrate after thoroughly cleaning the ITO sheets. Absorption spectra were recorded using Shimadzu 3101 spectrometer. The PL was measured using a home-assembled system consisting of a two-stage monochromator, a photomultiplier tube (PMT) with a lock-in amplifier for PL detection, and an Ar^{+} ion laser operating at 488 nm and 5 mW (corresponding to 0.125 W cm^{-2}) for excitation in all the measurements. Fourier transform infrared (FTIR) spectra were recorded by Perkin Elmer Instrument (Spectrum BX-500).

Results and discussion

Colour gradation upon UV exposure

Figure 1a–e shows color photographs displaying wide spectral range of luminescence under 365 nm UV exposure from PPV polymer, CdSe nanocrystals, and PPV–CdSe composites dispersed in pyridine and toluene solvents, respectively. However, PPV in pyridine exhibits much brighter and uniform luminescence displaying orange color, whereas PPV in toluene displays pink color of less intensity, and color gradations are observed (Fig. 1a,b). On the other hand, CdSe nanocrystals dispersed in toluene displays much brighter uniform luminescence exhibiting intense blue color as compared to faint, non-uniform blue color exhibited upon its suspension in pyridine (Fig. 1c,d). The TOP/TOPO species, which perfectly passivates the CdSe nanocrystals gets stripped off due to pyridine, thus leaving bare CdSe nanocrystals suspended in pyridine, and hence, this color-graded variation of CdSe in different solvents (pyridine and toluene) can be understood. However, from Fig. 1e, for PPV–CdSe composites suspended in pyridine, its luminescence is mainly dominated by PPV (although concentration of CdSe nanocrystals ~60% by weight), exhibiting similar uniformity and color of emission as shown in Fig. 1a.

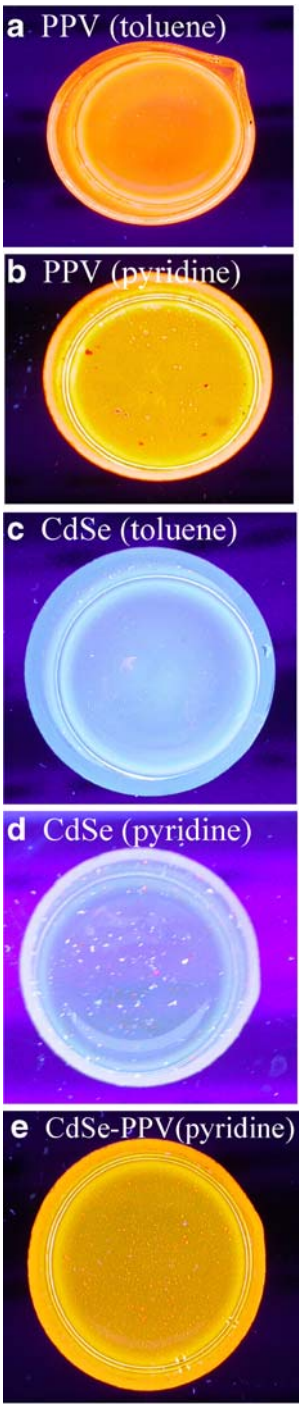

Fig. 1 Color photographs depicting the luminescence of MEH-PPV (**a**,**b**), CdSe (**c**,**d**), and PPV–CdSe (**e**) nanocomposites in toluene and pyridine solvents

The absorption and emission spectra of poly[2-methoxy-5-(2′-ethyl-hexyloxy)-1,4-phenylene vinylene] (MEH-PPV) in toluene are shown in Fig. 2a. In the spectrum of pure PPV (Fig. 2a, curve a), there is a major broad absorption peak centered at 500 nm. The peak of emission of PPV in toluene is at about 560 nm with a shoulder at about 595 nm (Fig. 2a, curve b). Figure 2b (curves a and b) shows absorption band ~495 nm and emission peak at ~570 nm for PPV polymer in pyridine solvent. On comparing Fig. 2a,b (curve a), it is evident that there is a difference in emission maximum ($\lambda_{max}\pm10$ nm) of PPV in different solvents (toluene and pyridine). Moreover, the intensity of the prominent emission shoulder ~595 nm as exhibited by PPV in toluene solvent (Fig. 2a, curve b) gets drastically reduced when PPV is suspended in pyridine. These results are in accordance with the earlier reported, where a slight red shift of absorption spectra of PPV in aromatic solvents (Triton X-100) compared with that in aliphatic solvents (toluene) is obtained [35]. This difference is clearer in emission spectra, which are narrower and well defined. It is known that the absorption and emission spectrum of conjugated polymer depends on its molecular conformation due to the changing conjugation length of the polymer [35, 36]. Thus, it is expected that PPV polymer might have different conjugation length in different solvents [35, 36]. Thus, from the absorption and emission intensity profiles of PPV in different solvents of toluene and pyridine, such trend is evident. Our results are in accordance with the findings of Diaz-Garcia et al. [37] where photophysics of MEH-PPV polymer films cast from different solvents were found to be different. Figure 2c shows the absorption and PL spectra of CdSe nanocrystallites (Cd/Se, ~2:1) in pyridine solvent. The inset of Fig. 2c shows the absorption (λ_{abs}, ~485 nm) and emission (λ_{PL}, ~510 nm) profiles of CdSe in toluene solvent. Here, the sharp absorption features

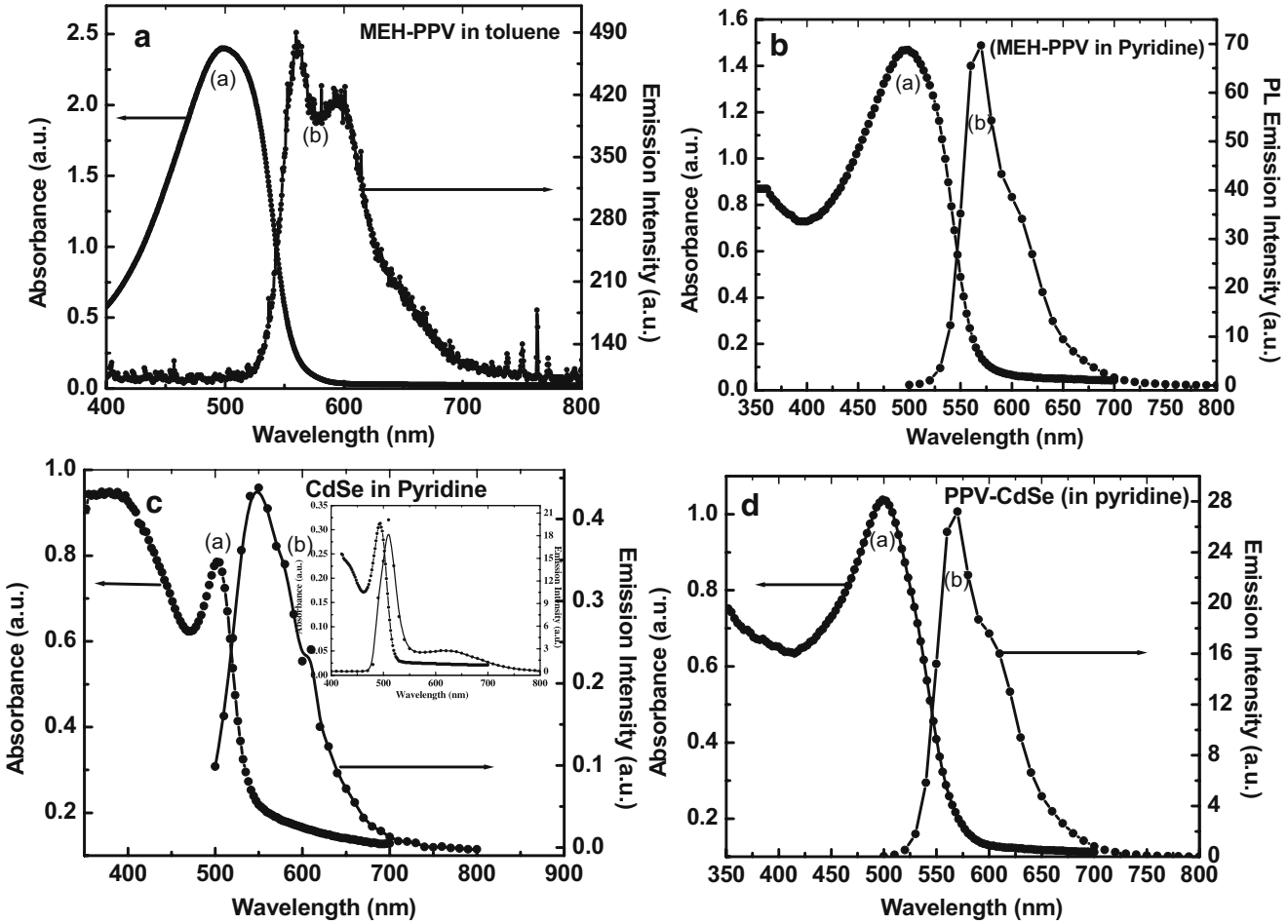

Fig. 2 Absorbance and emission spectra of MEH-PPV (**a**,**b**), CdSe (**c**), and PPV–CdSe (**d**) nanocomposites in pyridine and toluene solvents. Inset of **c** represents absorbance and emission spectra of ~5 nm CdSe QDs in toluene

and narrow emission profile indicate band-edge emission and high monodispersity. Both absorption and PL spectra corresponding to CdSe nanocrystals in different solvents (toluene and pyridine) exhibit the strong quantum size effects vide [38]. For these quantized nanoparticles, as can be seen from Fig. 2c, the red shift in the edges of the absorption band from 533 to 543 nm and PL band from 510 to 549 nm on changing the solvent from toluene to pyridine simply demonstrates that desorption of capping agent TOP/TOPO species by pyridine leads to agglomeration of CdSe nanoparticles, and hence, an increase in particle size is observed. The significant increment in full width at half-maximum (FWHM) of emission profile corresponding to CdSe in pyridine as compared to that in toluene indicates broad size distribution of nanoparticles. Figure 2d shows absorption and emission spectra of PPV–CdSe composites in pyridine solvent. As evident from Fig. 2d, the emission and absorbance characteristics of the composites are clearly dominated by PPV (λ_{ABS}, ~500 nm; λ_{PL},~570 nm) as also supported from their corresponding UV photographs (Fig. 1b,e). Furthermore, Fig. 2d (curve b) shows clearly the PL quenching of MEH-PPV in the addition of CdSe nanocrystals in pyridine solvent, indicating that the charge transfer has taken place.

Figure 3a,b shows the emission intensity profile of PPV–CdSe composite in toluene solvent as a function of volume of CdSe with different nanocrystalline diameters 5 and 7 nm, respectively. As evident in Fig. 3a,b, there is no systematic pattern of either increase or decrease in the emission intensity of PPV–CdSe composite with an increase in concentration of CdSe nanocrystallites in toluene solvent. However, for PPV–CdSe composites in pyridine solvent, a systematic decrease in emission intensity of PPV–CdSe composite is observed with increase the in CdSe concentration, as shown in Fig. 4a–c. This is because of the fact that TOP/TOPO species, which is a capping agent for CdSe nanocrystallites, prevents its interaction with PPV. When the surface TOP/TOP species is removed by treatment with pyridine, however, there is a significant quenching of emission intensity of PPV–CdSe composites, implying that the removal of TOP/TOPO groups allows electron transfer to occur, leading to the formation of separated electron-hole

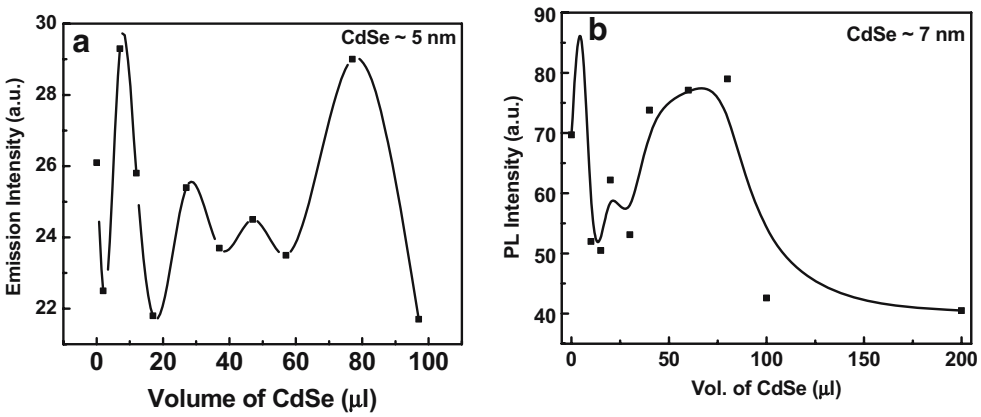

Fig. 3 Emission intensity profile of PPV-nanoparticle composites in toluene as a function of volume of CdSe. **a** CdSe (5 nm) and **b** CdSe (7 nm)

pairs that subsequently recombine nonradiatively. It is important to note here that the quenching of the polymer luminescence, while significant, is not complete even at high nanocrystal concentrations (Fig. 4c). This could be due to the occurrence of phase segregation in the composite material; if the CdSe nanocrystals were randomly dispersed in the PPV matrix, absolute complete quenching could have been expected.

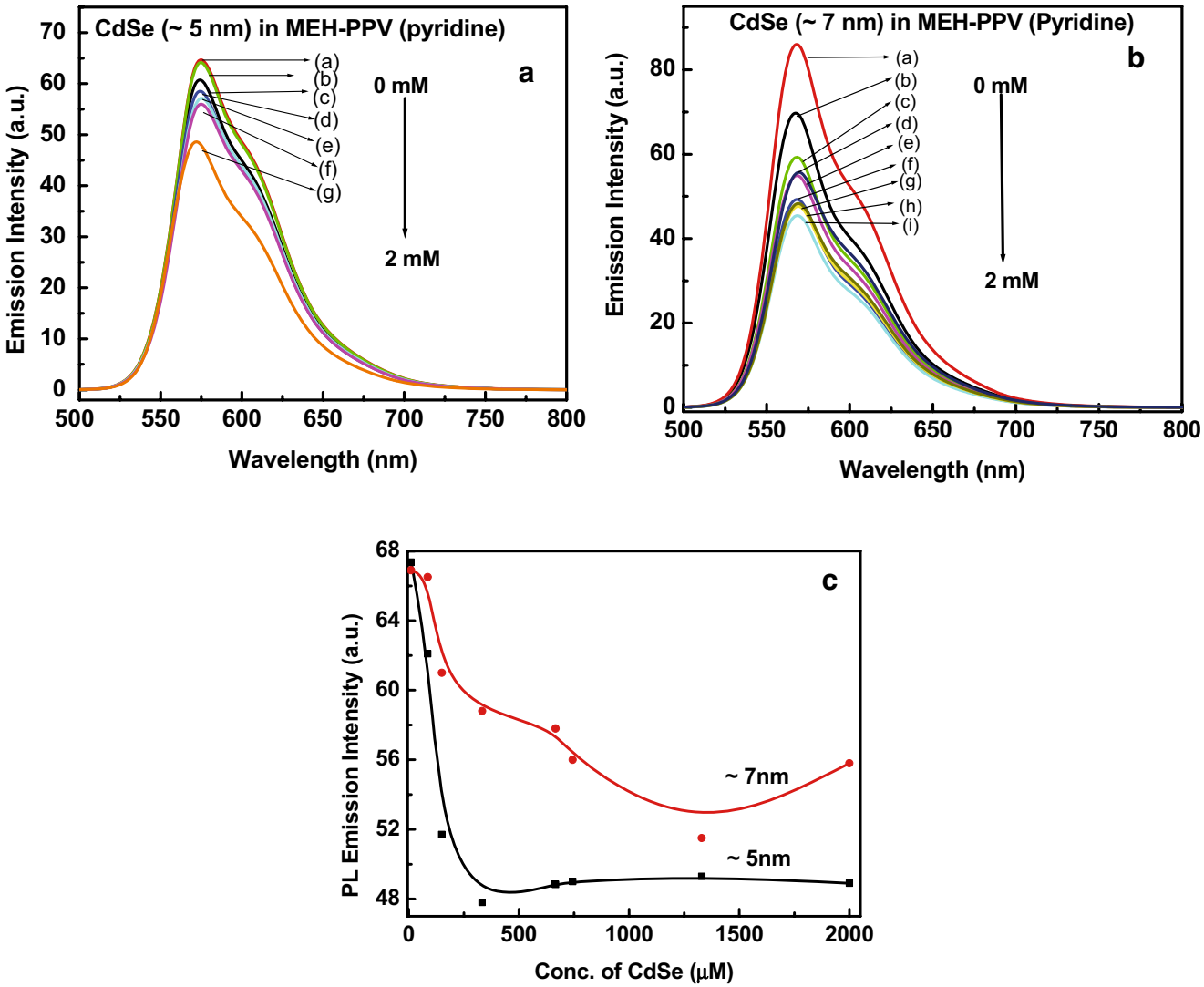

Fig. 4 Emission intensity profiles of PPV-nanoparticle composites in pyridine. **a** CdSe (5 nm) in the presence of CdSe at different concentrations: *(a)* 0, *(b)* 0.1, *(c)* 0.2, *(d)* 0.5, *(e)* 0.8, *(f)* 1.0, *(g)* 1.2 *(h)* 1.5, and *(i)* 2 mM, respectively. **b** CdSe (7 nm) in the presence of CdSe at different concentrations: *(a)* 0, *(b)* 0.1, *(c)* 0.2, *(d)* 0.5, *(e)* 0.8, *(f)* 1.0, *(g)* 2 mM, respectively. **c** Profile as a function of concentration of CdSe for different sized CdSe nanoparticles

Luminescence quenching refers to any process that decreases the luminescence intensity of a sample. There are two basic types of quenching: static and dynamic or (collisional) [39]. Both types require an interaction between the fluorophore and quencher. In the case of dynamic quenching, the quencher must diffuse to the fluorophore during the lifetime of the excited state. Upon contact, the fluorophore returns to the ground state without emission of a photon [39]. In the case of static quenching, a complex forms between the fluorophore and the quencher, and this complex is nonfluorescent. The formation of this complex does not rely upon the population of the excited state [39].

In the simplest case of collisional quenching, the following relation, called the Stern–Volmer equation [39], holds:

$$\frac{I_0}{I} = 1 + K_{SV}[Q] \quad (1)$$

where I_o and I are the fluorescence intensities observed in the absence and presence, respectively, of quencher, $[Q]$ is the quencher concentration, and K_{SV} is the Stern–Volmer quenching constant. In the simplest case, then a plot of I_o/I vs $[Q]$ should yield a straight line with a slope equal to K_{SV} [39]. Such a plot known as a Stern–Volmer plot is shown as Fig. 5a (curves a and c) in the case of quenching of emission of PPV polymer–CdSe composites with increase in concentration of CdSe nanocrystallites of diameters 5 and 7 nm, respectively. However, as evident in Fig. 5a,c, nonlinear Stern–Volmer plots with negative deviation from linearity are obtained. Such nonlinear Stern–Volmer plots can occur in the case of heterogeneous quenching (collisional or static) if some of the fluorophores are less accessible than others [39, 40]. From Fig. 5 (curves a and c), the similarity in the Stern–Volmer plots for PPV–CdSe composites corresponding to 5 and 7 nm of CdSe nano-

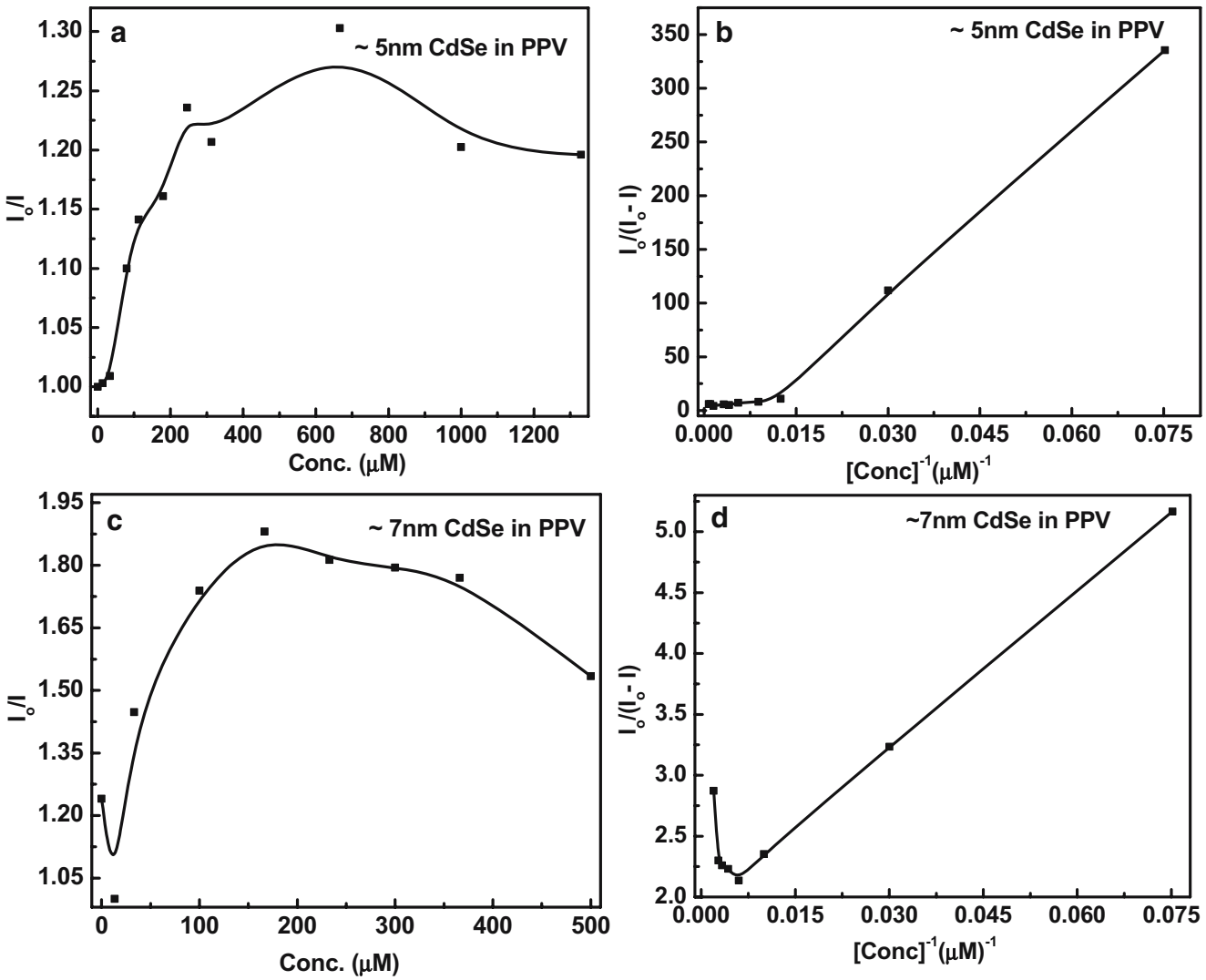

Fig. 5 Stern–Volmer plots of PPV–CdSe nanocomposites **a** CdSe (5 nm), **c** CdSe (7 nm), and modified Stern–Volmers (**b**, **d**) of corresponding CdSe

crystallites clearly indicates the presence of heterogeneous quenching due to the presence of accessible and inaccessible set of fluorophores, respectively. The heterogeneous quenching could be a result of insufficient coverage of polymers on the surface of CdSe nanocrystallites due to phase segregation for pyridine-treated CdSe. This effect would be felt more for broad-sized distribution of CdSe nanocrystallites of larger size of ~7 nm as compared to the smaller one of ~5 nm. This heterogeneous quenching and fractional accessibility have also been observed in the case of amines-treated CdSe nanocrystallites [41] and iodide quenching of tryptophan residues, respectively [40, 42].

Figure 5 (curves b and d) shows a modified Stern–Volmer plots of $I_o/\Delta I$ vs $1/[Q]$ for PPV–CdSe composites at different concentration $\{Q\}$ of CdSe nanocrystallites of sizes 5 and 7 nm, respectively. As shown in Fig. 5b, for smallest sized of ~5 nm CdSe nanocrystallite, linear Stern–Volmer plots are obtained with two slopes throughout the range of concentration of CdSe nanocrystallites in pyridine solvent. However, the corresponding modified Stern–Volmer plots for larger ~7-nm-sized CdSe nanocrystallites show linearity only at lower concentrations, as higher concentrations phase of CdSe nanocrystallites would encourage phase segregation. This explains nonlinearity of modified Stern–Volmer plots at higher concentrations of larger-sized (~7 nm) CdSe nanocrystallites (Fig. 5, curve d).

From above, it is not clear whether it is the static or dynamic quenching that is responsible for the decrease in emission intensity of PPV polymer upon addition of CdSe nanocrystals. Additional information is required to distinguish between the two, for example, absorption spectra and the lifetime dependence. In dynamic quenching, charge transfer occurs, and the fluorescence is quenched when the electron acceptor collides with the excited fluorophore. By careful examination of the absorption spectrum, one can attempt to distinguish static and dynamic quenching. Because the collision between the quencher and the fluorophore affects only the excited state of the fluorophore, no changes in the absorption spectrum are expected [39, 43]. On the contrary, the formation of ground-state complex in static quenching will perturb the absorption spectra of the fluorophore [39, 43]. Figure 6a–c shows the absorbance profiles of PPV, CdSe (size, ~7 nm) and PPV–CdSe composites in pyridine solvent. For comparison, the absorbance profile of PPV–CdSe (21) is also plotted (Fig. 6, curve d). Figure 6 clearly shows that the absorption spectrum of the mixture of PPV–CdSe composite is simply a linear combination of the spectra of each component, thus implying the presence of dynamic quenching. The data are consistent with the results of Zheng et al. [44]; even at the very high concentration of C60 in MEH-PPV mixture, they found neither spectral shift nor any new absorption band due to the complex formation. From Fig. 6, the position of the absorption edges for pure PPV, CdSe(31), PPV–CdSe (31) and PPV–CdSe(21) composites are found to be at ~568, 554, 588, and 575 nm, respectively. The higher absorption edge values for PPV–CdSe (31) as compared to PPV–CdSe (21) composites and pure PPV polymer in pyridine imply larger particle size indicating phase segregation or particle aggregation for the former than for the latter.

For further confirmation, TEM micrographs were taken for PPV–CdSe composites corresponding to 5- and 7-nm CdSe nanocrystallites (wt%, ~70%), respectively (Fig. 7a,b). From Fig. 7, it could be seen that even in the case of 5-nm-sized CdSe nanocrystallite blends, the CdSe QDs aggregated together to form predomain regions of densely packed nanocrystals surrounded by regions of MEH-PPV polymer. For larger CdSe crystallite sizes (~7 nm) with similar wt%, the densely packed QDs aggregate together increasingly. Transmission electron microscopy (TEM) images of polymer in pyridine-coated CdSe QDs blends show that the driving force for phase segregation seems to be the difference of polarity between the relative polar pyridine-coated CdSe QDs and the relative nonpolar MEH-PPV polymer. In recent studies, it has been observed that TEM images of PPV polymer in TOPO-capped CdSe QDs show that this aggregation of particles seems to be driven by van der Waals interactions between the CdSe QDs [45]. With these reasons, the blends of pyridine-coated CdSe QDs with PPV polymer would exhibit more aggregation as compared to TOPO-capped CdSe QDs–PPV blends.

Fourier transform infrared data for poly(p-phenylinevinylene)

Figure 8a–c shows FTIR transmittance spectra of pure PPV and PPV–CdSe composites corresponding to CdSe nanocrystallite of sizes ~5 and 7 nm in pyridine solvent, respectively. Figure 8a shows that pure PPV exhibits

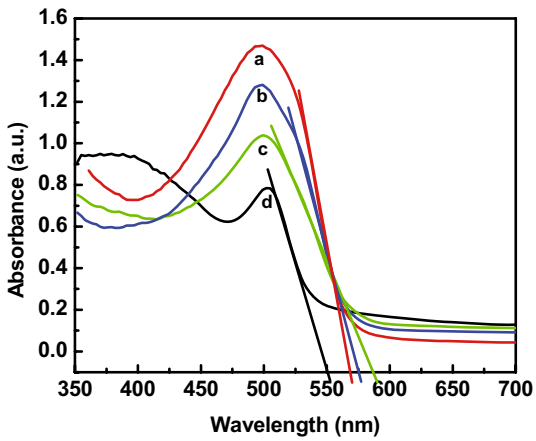

Fig. 6 Absorbance profiles of **a** PPV, **b**, **c** CdSe; PPV–CdSe composites (size, ~7 nm), and **d** PPV–CdSe composites (size, ~5 nm) in pyridine solvent

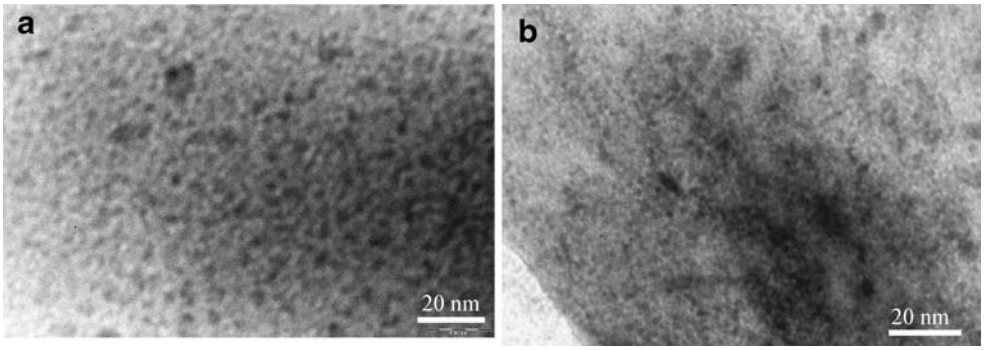

Fig. 7 TEM micrographs for PPV–CdSe nanocomposites corresponding to **a** 5 nm and **b** 7 nm CdSe nanocrystallites (wt%, ~70%)

doublet at ~3,089 cm^{-1} and 3,040 cm^{-1}, which is assigned to the trans-vinylene C–H stretching mode; a peak at ~2,365 cm^{-1} corresponds to C–H bending modes; peak at ~1,588 cm^{-1} is assigned to C–C ring stretching mode; and peaks at ~1,445 and 1,038 cm^{-1} are related to pyridine, respectively [46–48]. PPV–CdSe composites (CdSe nanocrystallite sizes, ~5 and 7 nm) in Fig. 8b,c exhibits similar peaks: 2,362 cm^{-1} corresponding to C–H bending modes; peaks at ~1,702 cm^{-1} correspond to C=O stretching modes; 1,538 and 1,558 cm^{-1} peaks correspond to pyridine-related modes that are bounded to CdSe nanocrystals, respectively [46, 47, 49]. From Fig. 8c, the small TOP/TOPO peak at ~1,454 cm^{-1} corresponding to PPV–CdSe composite for CdSe nanocrystallite of size ~7 nm suggests that even after ligand exchange with pyridine, the CdSe is still partially capped by TOP/TOPO. This feature is absent in the case of PPV–CdSe composite corresponding to 5-nm CdSe nanocrystallite (Fig. 8b). This partial capping by TOP/TOPO species for CdSe nanocrystallite (size, ~7 nm) explains the partial quenching of PPV–CdSe composites even at the highest concentration of CdSe as compared to that for smaller nanocrystallite (~5 nm) case.

Studies of thin films

Figure 9 (curves a–e) shows emission intensity profiles of PPV/ITO and PPV–CdSe/ITO composite films at different ratios of polymer/CdSe (PPV/CdSe). In the case of pure MEH-PPV, the main emission peak is ~593 nm with a hump at ~630 nm, respectively (Fig. 9, curve b). Pure CdSe (31) shows emission at ~579 nm (Fig. 9, curve a). For clarity, pure CdSe emission has been shown as inset in Fig. 9. As found in the case of solutions, the emission intensity of PPV–CdSe composites decreases with the increase in CdSe concentration. On increasing the CdSe concentration in the PPV–CdSe composites from 1:1 to 1:7, the peak emission intensity decreases with concurrent decrease in the emission hump at ~630 nm. At the highest CdSe concentration in PPV, i.e., PPV/CdSe of 1:7, there is hardly any discernible change in the emission (λ_{max} emission, ~590 nm). During the surface exchange of nanoparticles from TOP/TOPO to pyridine, the CdSe nanoparticles loose their luminescence because pyridine binds to the nanoparticles as hole trap, thereby removing these sites from participation in radiative electron hole recombination at the surface. For PPV–CdSe composites both in solutions and in thin film form, significant quenching of the

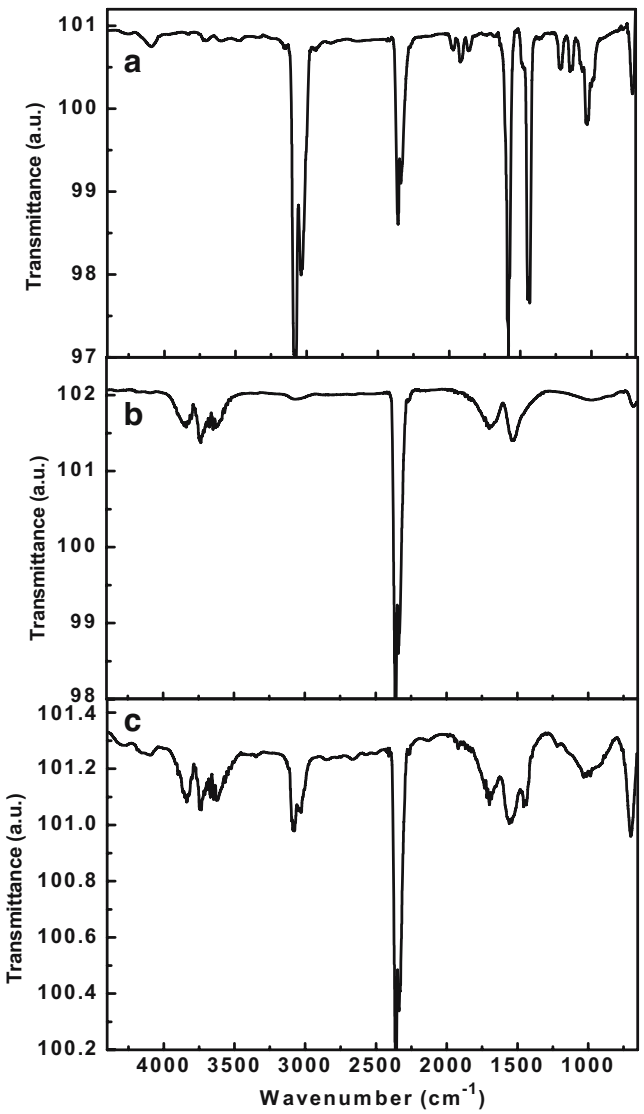

Fig. 8 FTIR transmittance spectra of **a** pure PPV and **b**, **c** PPV–CdSe composites corresponding to CdSe nanocrystallite of sizes of ~5 and 7 nm in pyridine solvent, respectively

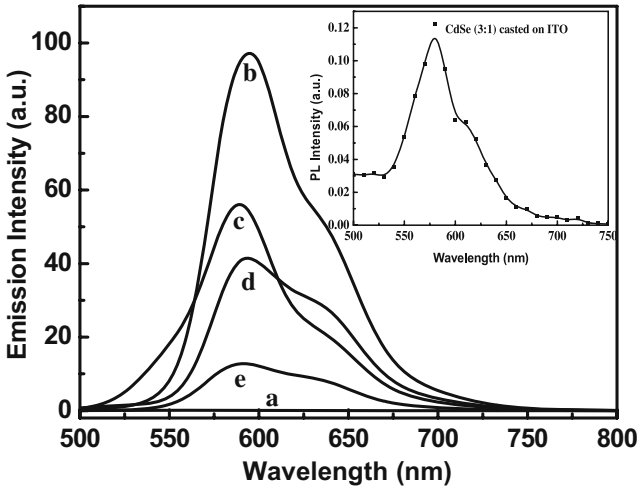

Fig. 9 Emission intensity profiles of PPV/ITO and PPV–CdSe/ITO composite films at different ratios of polymer/CdSe (PPV/CdSe); **a** (*inset*) pure CdSe (5 nm), **b** pure PPV, **c** PPV/CdSe (1:1), **d** PPV/CdSe (3:1), **e** PPV/CdSe (7:1)

luminescence takes place, indicating that charge transfer occurs at the polymer/nanocrystal interface. In comparing the emission intensity profiles of PPV in various solvents (toluene and pyridine; Fig. 2a,b, curves b) with that of solid state emission spectra (Fig. 9, curve b), it is interesting to note that PPV emission spectra in solid state is significantly red-shifted as compared to PPV solution spectra. This is due to the fact that the emitting species for the two polymers are different in various solvents and in the solid state [50]. A red shift in the emission on going from solution to solid state is commonly observed for polymers and is attributed to the increased conjugation length from improved ordering in the solid state [50]. From the emission intensity profiles of PPV both in solutions (toluene and pyridine) and in solid-state, it has been reported that the shape of the emission spectrum of polymers is determined by the nature of the emitting species and the amount of inhomogeneous broadening [51, 52]. Inhomogeneous broadening is due to the emission from a range of conjugation lengths in the sample, which has been observed in our case for both in solutions and in solid film form.

Quenching in PPV/ITO thin films upon addition of CdSe nanocrystals appears to be stronger as compared to their counterparts in solution form. This could be due the fact that PPV has significant crystallinity in the solid state and, as a result, has the most structured emission spectra with well-defined vibronic features [51]. Upon removal of the TOP/TOPO species, the nanocrystals agglomerate, and thus in PPV-CdSe composites, small islands of nanocrystals, which are separated from each other as also observed by TEM for composites in pyridine, result in an inefficient percolation network for charge transport.

In composites of PPV–CdSe both in solutions and in film form, PPV polymer dominates the PL emission spectra, and the luminescence contribution from quantum dots is not apparently evident. While the quantum yield of PPV is expected to diminish when going from solution to the solid state due to self-quenching [53]. However, in the solid-state PL spectrum of the composite, the PPV emission still dominates. According to other studies, high loadings of quantum dots (50%) or greater are typically needed to observe quantum dot emission in quantum-dot-conducting polymer blends. We suppose that in our case of PPV–CdSe nanocrystallite composites, the presence of substantial nanoparticle aggregation, as demonstrated by TEM results, limits interfacial contact between the polymers and quantum dots, thus limiting charge or energy transfer pathways and furthermore leading to self-quenching of nanoparticle luminescence emission. The phase segregation would lower the quantum efficiency of PPV–CdSe composites due to poor transport of charges. Therefore, efforts should be made to improve the film morphology of PPV–CdSe composites for its practical application in solid state devices.

As the absorption coefficient of CdSe nanocrystals is much smaller than that of MEH-PPV, even at the highest concentration of CdSe, and there is no overlap between the polymer emission spectrum and the nanocrystal absorption spectrum, there does not exist the possibility of Forster exciton transfer from polymer to nanocrystal [54]. Thus PL decrease in polymer upon addition of nanocrystals could be attributed to charge transfer rather than energy transfer from polymer to nanocrystal.

Polystyrene

The emission spectrum of pristine polystyrene (10 wt%) in toluene is shown in Fig. 10a. In the spectrum of pure polystyrene, a weak and broad peak of emission of polystyrene is at about 536 nm with a shoulder at about 564 nm (Fig. 10a). Figure 10b shows the PL spectra of pure CdSe nanocrystallites (size, ~7 nm) and CdSe in 10% polystyrene (10 wt%) in toluene solvent. Pure CdSe nanocrystallite exhibits an emission peak at ~521 nm while the one dispersed in 10 wt% polystyrene shows emission at ~518 nm. A slight blue shift (~3 nm) is observed with concomitant broadening of PL peak half width (FWHM) upon introduction of polymer into CdSe solution. Similarly for 5 nm CdSe nanocrystallite, there is a blue shift in PL position from 510 to 507 nm with FWHM of the PL band remaining almost the same upon introduction of 10 wt% polymer into CdSe solution (Fig. 10c, curves a and b). It should be noted that 5 nm CdSe nanocrystallite exhibits narrow emission profile and negligible surface states between 600–700 nm as compared to 7 nm CdSe nanocrystallite. However, a significant drop in PL intensity (both PL CdSe exciton and surface state) upon introduction of polymer into CdSe is prominent for 7 nm as compared to

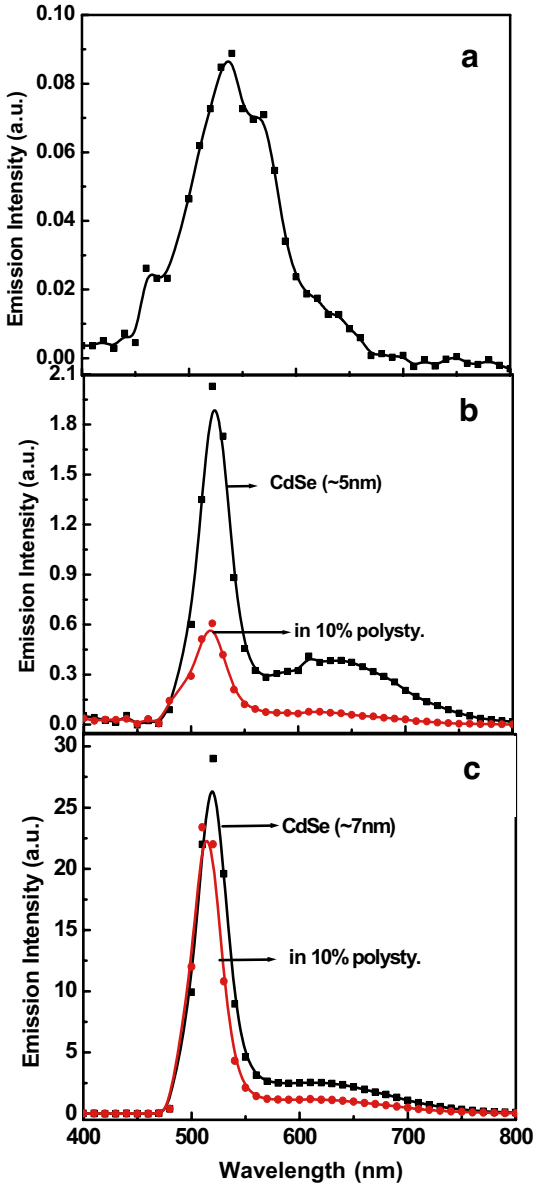

Fig. 10 Emission profiles 10 wt% polystyrene and polystyrene–CdSe composites. **a** Pure polystyrene; **b** polystyrene–CdSe, ~5 nm; **c** polystyrene–CdSe, ~7 nm

5 nm CdSe nanocrystallite. Furthermore, Fig. 10b,c shows clearly the PL quenching of CdSe upon addition of polymer in toluene solvent, indicating that the charge transfer has taken place. Although here, toluene instead of pyridine is used as the solvent, still quenching of CdSe emission by polymer, i.e., charge transfer, takes place. This indicates that interaction between CdSe and polymer can occur only after the removal of TOP/TOPO species from the surface of CdSe nanocrystallites. However, in some cases, it has been observed that even with TOPO intact, charge transfer has taken place. This would be further cleared in subsequent sections.

Figure 11a shows a weak emission spectrum of pure polystyrene (20 wt%) with $\lambda_{emission}$ of ~530 nm with shoulder at ~560 nm similar to that for pure polystyrene 10 wt% (Fig. 10a). Upon addition of polymer into CdSe solution (nanocrystallite size, ~7 nm), there is a shift in CdSe emission from 524 to 519 nm, with significant drop in PL intensity similar to that observed for the corresponding CdSe–polystyrene (10 wt%; Fig. 10b). Similarly for CdSe nanocrystallite size of ~5 nm, there is a blue shift in emission peak from 510 to 501 nm with a drop in

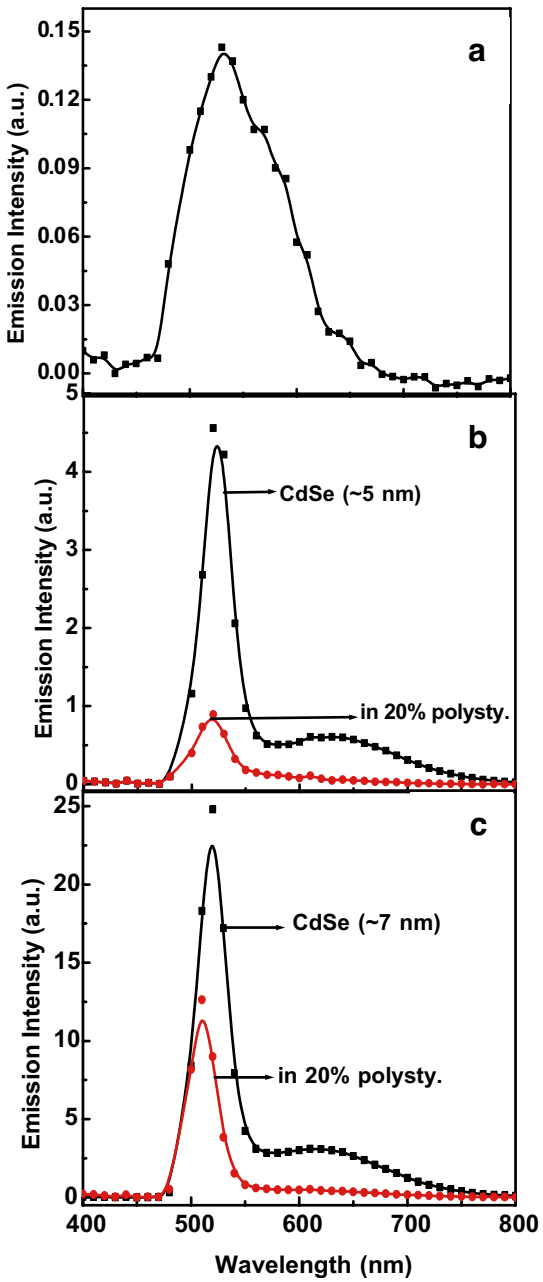

Fig. 11 Emission profiles 20 wt% polystyrene and polystyrene–CdSe composites. **a** Pure polystyrene; **b** polystyrene–CdSe, ~5 nm; **c** polystyrene–CdSe, ~7 nm

PL intensity upon addition of polymer into CdSe solution (Fig. 11b). Thus, with the increase in weight percent of polystyrene from 10 to 20, a higher blue shift is observed for both 7- and 5-nm CdSe nanocrystallites. With further increase in weight percent of polystyrene to 40 wt%, pure polystyrene exhibits similar weak emission at ~536 nm (Fig. 12a). Here, the corresponding CdSe nanocrystallites (7 and 5 nm) exhibits similar reduction in emission intensity and emission blue shift from 521 to 518 (i.e., 3 nm) and from 510 to 502 nm (i.e., 8 nm) respectively (Fig. 12b,c).

Figure 13a,b shows spectra of PL intensity and FWHM of PL band as a function of % wt of polystyrene. The smaller CdSe nanocrystallite (size ~5 nm) exhibits a sharp decrease in PL intensity with almost similar FWHM with an increase in weight percent of polystyrene (Fig. 13a, curve a). However, in case of larger CdSe nanocrystalite (size, ~7 nm), the PL intensity does shows a decreasing trend but to a lesser extent as compared to that of smaller CdSe nanocrystallite (~size of 5 nm; Fig. 13a). Here, the surprising trend is the continuous increase in FWHM values for PL band with an increase in weight percent of polystyrene (Fig. 13b). Thus, for larger CdSe nanocrystallite, charge transfer is less while increase in FWHM values indicates increment in disorder, whereas smaller CdSe nanocrystallite shows efficient charge transfer process (maximum quenching observed) and remains stable with an increase in weight percent of polystyrene.

From the above results, it can be inferred that CdSe–polystyrene composite solutions shows a blue shift in PL with concurrent drop in PL intensity. The blue shift in PL can be attributed to a slight decrease in particle size during TOPO removal or exchange process by polystyrene, which could lead to stripping of CdSe as well. However, the significant drop in PL intensity for CdSe–polystyrene composite solutions clearly indicates that charge transfer from polymer to CdSe nanocrystals takes place as also observed in the case of conducting polymer PPV–CdSe composites. Stable polystyrene–CdSe composites with maximum charge transfer efficiency is obtained for smaller CdSe nanocrystallite as compared to the larger one. Steric hindrance due to larger particle size and phase segregation as observed in the case of PPV–CdSe composites could be the factors responsible for limiting charge transfer efficiency for larger CdSe nanocrystallites (~7 nm).

In an earlier work [27], it was observed that CdSe nanoparticles dispersion in toluene and polystyrene does not have any effect on the emission peak position (~580 nm). This implies that CdSe nanocrystalline diameter practically remains unchanged regardless of the nature of the polymers [27]. In our case, CdSe nanocrystals of sizes 5 and 7 nm show a blue shift in emission intensity with increase in weight percent of polystyrene. This could

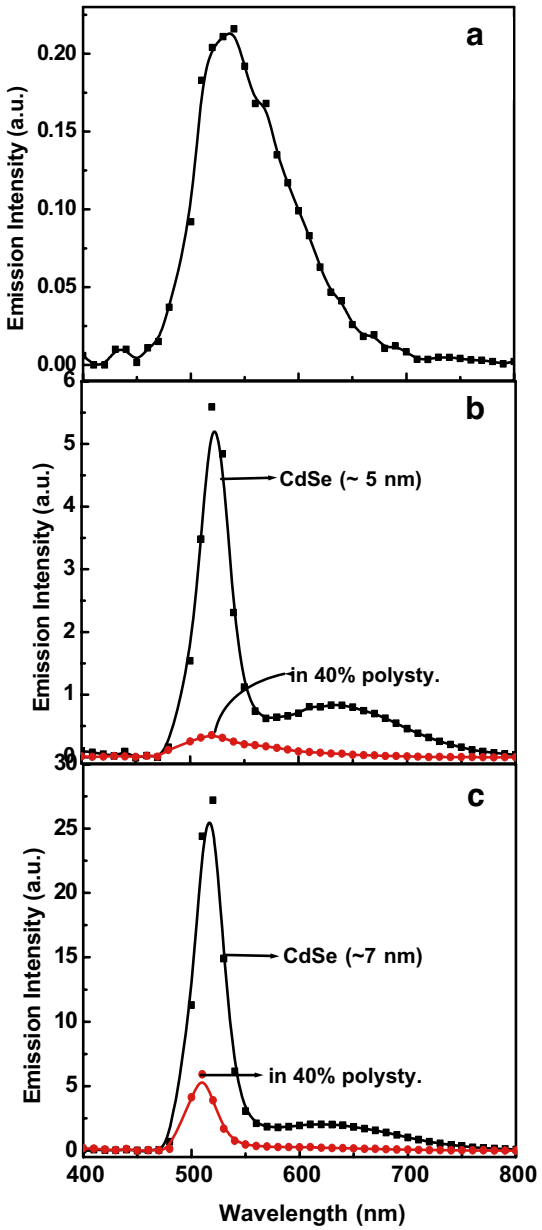

Fig. 12 Emission profiles 40 wt% polystyrene and polystyrene–CdSe composites. **a** Pure polystyrene; **b** polystyrene–CdSe, ~5 nm; **c** polystyrene–CdSe, ~7 nm

be due to the decrease in CdSe nanocrystallite size upon surface exchange of TOP/TOPO species by polystyrene polymer leading to stripping off the CdSe. These results are in sharp contrast to that obtained for PPV–CdSe composites, which showed particle-agglomeration leading to an increase in particle size and hence red shift in absorption edge and PL emission peak. In case of PPV–CdSe nanocomposites, the limiting mechanism for particle growth is probably the inhibition of diffusion, as the bending or coiled structures of the polymer chains will hinder the diffusion-driven processes within the network. It is also possible that polymer chains may be bridged by connecting

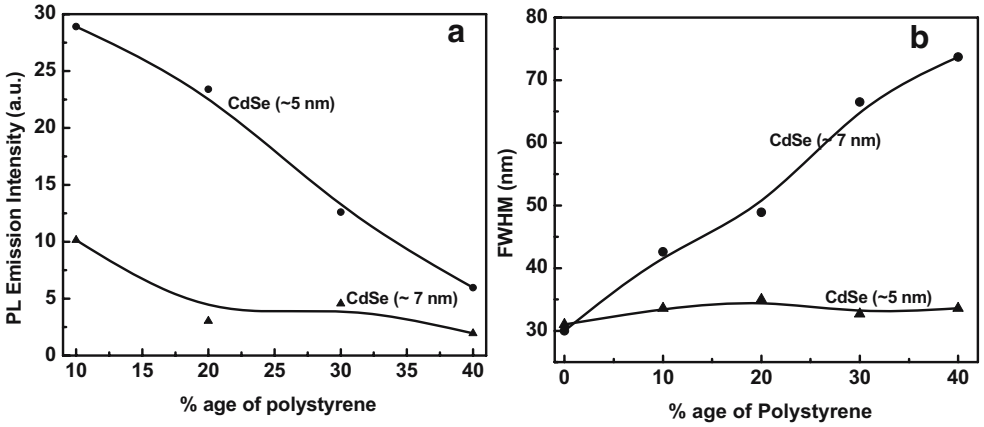

Fig. 13 **a** PL intensity and **b** FWHM of polystyrene–CdSe composites as a function of wt% of polystyrene

to the same nanoparticle, and a multiplicity of such bridged chains and particles could lead to particle clusterings. The PL red shift observed in the case of PPV–CdSe composites can also be reasonably attributed to reabsorption of the light emitted from the smaller nanocrystals by the larger ones within the same sample, together with a possible energy transfer between nanocrystals. However, as there is no overlap between the absorbance spectra of CdSe and emission spectra of PPV, energy transfer possibility can be excluded. Therefore, it can be said that for polystyrene–CdSe composites, morphological homogeneity of the CdSe nanocrystals is maintained in the final nanocomposites.

Emission spectra of the polystyrene–CdSe composites corresponding to 7-nm CdSe nanocrystalite size showed much broader bandwidths as compared to corresponding composites for 5-nm CdSe nanocrystallites. Higher FWHM values are most likely due to the wider particle size distribution or due to defects incorporated with the increase in weight percent of polystyrene. The broader particle size distribution is probably the consequence of a wide molecular weight distribution of the polystyrene polymer.

To probe the charge transfer across polystyrene–CdSe composites, FTIR transmittance spectra of pure polystyrene polymer and CdSe nanocrystallites (size, ~5 and 7 nm) in the absence and presence of polystyrene polymer were taken. For pure polystyrene FTIR spectra (Fig. 14a), a triplet band between 2,880–3,034, 2,364, and 724 cm^{-1} corresponds to CH-stretching (sp^3), CH-bending, and methylene ($–CH_2$) vibrational modes, respectively [48, 55, 56]. The 1,500 and 1,596 cm^{-1} peaks correspond to C=C ring-stretching modes [55]. The peak at ~1,736 cm^{-1} corresponds to C=O vibrational mode [56]. The peak at ~1,864 cm^{-1} is an overtone of the C–H stretching modes while the peak at ~724 cm^{-1} corresponds to C–H out-of-plane bending modes [56, 57] and 1,026 cm^{-1} corresponds to the ring in phase C–H stretching vibrations [56]. Figure 14b shows the FTIR transmittance spectra of pure CdSe (~5 nm), and it exhibits well-defined main peaks: triplet band between 2,880–3,100, 2,360, and 725 cm^{-1} corresponding to CH-stretching (sp^3), CH-bending, and methylene ($–CH_2$) vibrational modes, respectively [48, 56]. However, the presence of strong IR peak at ~1,490 cm^{-1} with a shoulder at 1,467 cm^{-1} corresponding to P=O stretching vibrational modes indicates the signatures of capping agent, i.e., TOPO/TOP bounded to CdSe nanocrystals respectively [57]. In case of 7-nm CdSe nanocrystallites, C–H bending modes are intense at ~2,359 cm^{-1} as compared to that of 5-nm CdSe nanocrystallite (Fig. 14c). However, for larger CdSe nanocrystallite (~7 nm), the signature of TOP/TOPO signals at ~1,512 cm^{-1} reduces as compared to that of smaller 5-nm CdSe crystallite (Fig. 14c). In the presence of polystyrene, the signature of TOPO/TOP transmittance signal becomes weaker at ~1,564 and 1,556 cm^{-1} indicating partial exchange of TOP/TOPO groups by polystyrene corresponding to CdSe nanocrystallites of sizes 5 and 7 nm, respectively (Fig. 14, curves d and e).

The CdSe–polymer composites were analyzed by scanning electron microscopy (SEM). Figure 15 shows representative SEM photographs of CdSe–polymer composites (size, ~5 nm) for polystyrene and PPV polymers, respectively. Figure 15a reveals that for CdSe–polystyrene composites; tiny particles are spread across the matrix. There appears to be unevenness in the film morphology, which could be due to the crystalline nature of the particles present in the polymer. Presence of spherical particles of CdSe is seen in the polymer matrix. However, in the case of CdSe–PPV composites (Fig. 15b), presence of agglomerated CdSe nanoparticles are indicated, resulting in irregular shape and morphology. The morphological quality of the CdSe–polymer composites that was obtained from polystyrene appears to be better than PPV.

Figure 16a,b shows the PL intensity spectra of polystyrene–CdSe and PPV–CdSe composites corresponding to 5- and 7-nm CdSe nanocrystallites, respectively, as a function of laser exposure time. Polystyrene–CdSe composite corresponding to 5-nm CdSe nanocrystallite shows steady behavior throughout the laser exposure (Fig. 16a, curve a). Here, the PL intensity does not change much and is

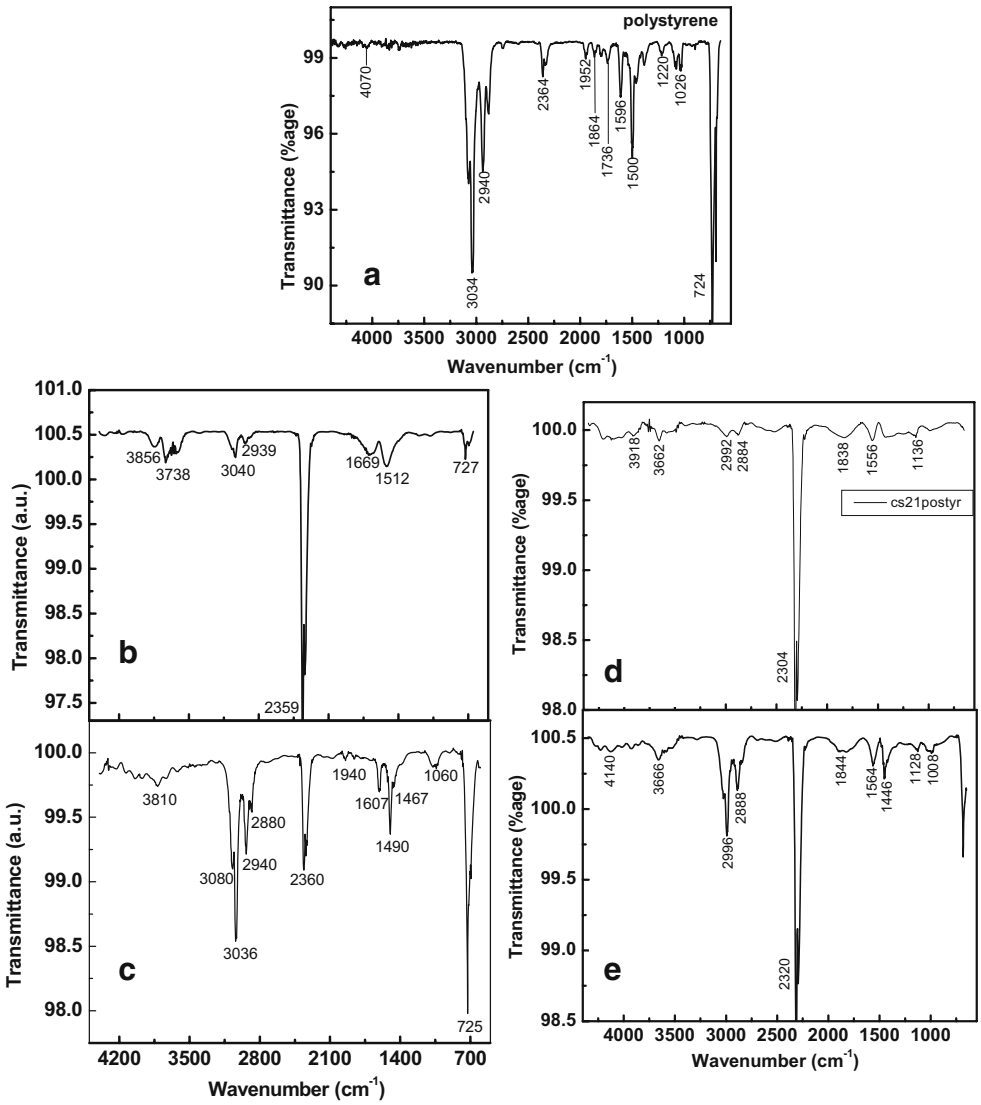

Fig. 14 FTIR transmittance spectra of polystyrene and polystyrene nanocomposites. **a** Pure polystyrene; **b**, **c** CdSe (~ 5 and 7 nm); **d**, **e** polystyrene nanocomposites (~ 5 and 7 nm)

virtually constant during the period of laser exposure. However, polystyrene–CdSe nanocomposite (~7 nm) shows steady behavior only after 20 min of laser exposure, as it shows initial decrease in PL intensity during the first 20 min of laser exposure (Fig. 16a, curve b). On the other hand, for PPV–CdSe composites corresponding to 5- and 7-nm CdSe nanocrystallite size (Fig. 16b), both shows enhancement in PL intensity upon laser exposure. In this case, the mechanism involved is either the adsorption of oxygen and/or water molecules, which reduces recombination

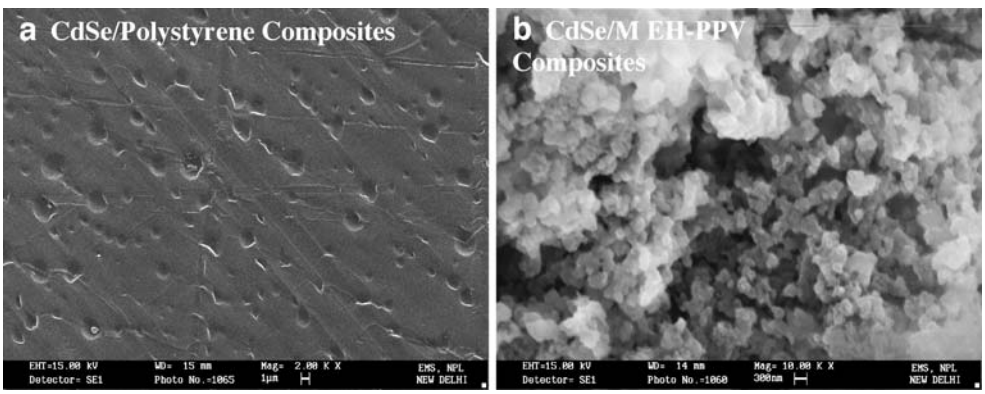

Fig. 15 SEM micrographs of polymer–CdSe nanocomposites (~5 nm); **a** polystrene–CdSe, **b** PPV–CdSe

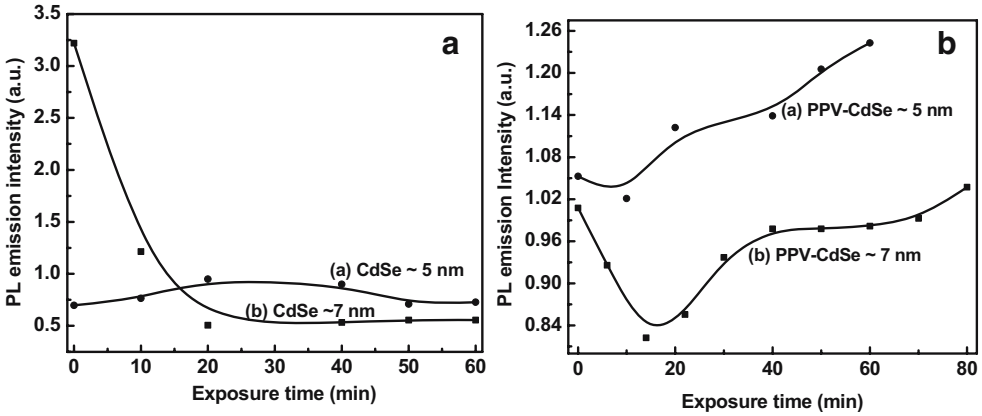

Fig. 16 PL degradation as a function of laser exposure time for polymer–CdSe nanocomposites. **a** Polystyrene–CdSe, **b** PPV–CdSe

from surface states, or a surface photo-oxidation, which can create an additional barrier for the carriers [58, 59]. Prolonged exposure to laser irradiation in the presence of oxygen inevitably results in photo-oxidation. It is to be noted here that for PPV–CdSe composite (~7 nm; Fig. 16b, curve b), the PL intensity initially decreases for first 15 min of laser exposure similar to that of corresponding polystyrene–CdSe composite. However, upon further laser exposure, the PL intensity shows a steady increase rather than decrease as observed in the case of PPV–CdSe composite. From the above results, it can be inferred that polystyrene–CdSe composites are much more stable than those of corresponding PPV–CdSe composites, which suggests that the polystyrene shield can effectively enhance the photostability of the CdSe QDs. This further implies that the hydrophobicity and compact structure of polystyrene polymer can effectively impede the diffusion of both oxygen and water from the surrounding environment into the polymer–CdSe composites, as the photo-oxidation of QDs is strongly coupled with the presence of oxygen and water. The early decrease in the PL intensity of both the polymer (polystyrene/PPV)–CdSe QDs corresponding to 7-nm CdSe nanocrystallite may be attributed to the photodegradation of the dots in the vicinity of the shallow surface of the composites.

Thus, in the case of polymer–CdSe composites corresponding to smaller and larger CdSe nanocrystallites, polystyrene–CdSe composites seems to have better structural and morphological properties as compared to PPV–CdSe composites mainly because of its short chain, which facilitates extensive coverage of nanocrystal surface due to reduced steric hindrance. For PPV–CdSe composites, it is mainly PPV that governs the optical properties of the composites even at the highest concentration of CdSe nanocrystallites. On the other hand, for polystyrene–CdSe composites, owing to poor emission of the polymer, properties are dependent on the concentration of CdSe nanocrystallites in the composites. However, for both the composites (PPV/polystyrene–CdSe), charge transfer between polymer and CdSe nanocrystallites does takes place resulting in quenching of emission of the respective host material.

Conclusions

The role of conducting (MEH-PPV) and nonconducting (polystyrene) polymers on the emission properties of CdSe nanocrystallites of varied sizes (5 and 7 nm) has been envisaged. The properties of PPV–CdSe composites are mainly governed by PPV even at the highest concentrations of CdSe nanocrystallites. Efficient PL quenching for PPV–CdSe composites in pyridine solvent corresponding to smaller CdSe nanocrystallite (~5 nm) indicates charge transfer. However, the presence of residual TOP/TOPO species and agglomeration or phase segregation effects for pyridine-treated CdSe nanocrystals restrict the PL-quenching mechanism particularly for larger sized (~7 nm) CdSe nanocrystallites as indicated by higher absorption edge values and TEM results. MEH-PPV polymer has been found to have different conjugation lengths in different solvents (toluene and pyridine) and in solid state form. Thus, for efficient charge transfer in PPV–CdSe composites, structural morphology, particularly for larger CdSe nanocrystallites, needs to be improved. Polystyrene polymer, on the other hand, also shows charge transfer across polymer–CdSe interface but, owing to its smaller chain length, has better surface coverage on the CdSe nanocrystallites as compared to PPV and renders photostability to CdSe QDs within the polymer matrix.

Acknowledgments We thank Director NPL for the encouragement to perform this work. The financial assistance from the Department of Science and Technology, New Delhi is gratefully acknowledged. Dr. SK Dhawan (Polymer Group, NPL) is greatly acknowledged for providing PPV and for his interest in this work.

References

1. Alivisatos AP (1996) Science 271:933
2. Yen BKH, Scott NE, Jensen KF, Bawendi MG (2003) Adv Mater 15:1858
3. Qu L, Peng X (2002) J Am Chem Soc 124:2049
4. Han M, Gao X, Su JZ, Nie S (2001) Nat Biotechnol 19:631
5. Tessler N, Medvedev V, Kazes M, Kan S, Banin U (2002) Science 295:1506
6. Murray CB, Norris DJ, Bawendi MG (1993) J Am Chem Soc 115:8706
7. Zhong X, Han M, Dong Z, White TJ, Knoll W (2003) J Am Chem Soc 125:8589
8. Qu L, Yu WW, Peng X (2004) Nano Lett 4:465
9. Hambrock J, Birkner A, Fischer RA (2001) J Mater Chem 11:3197
10. Battaglia D, Peng X (2002) Nano Lett 2:1027
11. Pyun J, Matyjaszewski K (2001) Chem Mater 13:3436
12. Huynh WU, Peng X, Alivisatos AP (1999) Adv Mater 11:923
13. Chen W, Joly AG, Malm JO, Bovin JO, Wang S (2003) J Phys Chem B 107:6544
14. Winiarz JG, Zhang LM, Lal M, Friend CS, Prasad PN (1999) J Am Chem Soc 121:5287
15. Dabbaousi BO, Bawendi MG, Onitsuka O, Rubner MF (1995) Appl Phys Lett 66:1316
16. Peng XG, Manna L, Yang WD, Wickham J, Scher E, Kadavamich A, Alivisatos AP (2000) Nature 404:59
17. Alivisatos AP (1996) J Phys Chem 100:13226
18. Ginger DS, Greenham NC (1999) Phys Rev B 16:10622
19. Caseri W (2000) Macromol Rapid Commun 21:705
20. Moffitt M, Vali H, Eisenberg A (1998) Chem Mater 10:1021
21. Antonietti M, Goltner C (1997) Angew Chem Int Ed Engl 36:910
22. Li X, Freyer JR, Cole-Hamilton DJ (1994) J Chem Soc Chem Commun 14:1715
23. Sankaran V, Yue J, Cohen RE, Schrock RR, Silbey R (1993) J Chem Mater 5:1133
24. Wang Y, Mahler W (1987) Opt Commun 61:233
25. Hilinski EF, Lucas PA, Wang Y (1988) J Chem Phys 89:3435
26. Yuan Y, Fendler JH, Cabasso I (1992) Chem Mater 4:312
27. Trindade T, Neves MC, Barros AMV (2000) Scripta Mater 43:567
28. Yang Y, Huang J, Liu S, Shen J (1997) J Mater Chem 7:131
29. Pavel FM, Mackay RA (2000) Langmuir 16:8568
30. Wang S, Yang S, Yang C, Li Z, Wang J, Ge W (2000) J Phys Chem B 104:11853
31. Bowen Katari JE, Colvin VL, Alivisatos AP (1994) J Phys Chem 98:4109
32. Sharma SN, Sharma H, Singh G, Shivaprasad SM (2006) Nucl Instrum Methods Phys Res B 244:86
33. Sharma H, Sharma SN, Singh G, Shivaprasad SM (2006) Physica E 31:180
34. Greenham NC, Peng X, Alivisatos AP (1996) Phys Rev B 54:17628
35. Zheng M, Bai F, Zhu DJ (1998) Photochem Photobiol A 116:143
36. Sharma SN (2006) Colloid Polym Sci 284:853
37. Diaz-Garcia MA, Hide F, Schwartz BJ, Andersson MR, Pei Q, Heeger AJ (1997) Synth Met 84:455
38. Bawendi MG, Steigerwald ML, Brus LE (1990) Annu Rev Phys Chem 41:477
39. Lakowicz JR (1999) Principles of fluorescence spectroscopy, 2nd edn. Kluwer, New York
40. Samworth CM, Esposti MD, Lenaz G (1988) Eur J Biochem 171:81
41. Sharma SN, Sharma H, Karar N, Chandra H, Singh G, Shivaprasad SM (2007) Mater Chem Phys (in press)
42. Wyatt WA, Bright FV, Hieftje GM (1987) Anal Chem 59:2272
43. Birks JB (ed) (1975) Organic molecular photophysics. Wiley, New York, p 409
44. Zheng M, Bai F, Fengying L, Li Y, Zhu D (1998) J Appl Polym Sci 70:599
45. Shiang JJ, Kadavanich AV, Grubbs RK, Alivisatos AP (1994) J Phys Chem 99:17417
46. Deacon GB, Green JHS (1968) Spectrochim Acta 24a:845
47. Becerra LR, Murray CB, Griffin RG, Bawendi MG (1994) J Chem Phys 100:3297
48. Kalsi PS (2002) Spectroscopy of organic compounds. New Age International Pvt., New Delhi, p 60
49. Kim BS, Avila L, Brus LE, Herman IP (2000) Appl Phys Lett 76:3715
50. Gettinger CL, Heeger AJ, Drake JM, Pine DJ (1994) J Chem Phys 101:1673
51. Martens JHF (1993) Synth Met 55–57:434
52. Harrison NT, Baigent DR, Samuel IDW, Friend RH, Grimsdale AC, Moratti SC, Holmes AB (1996) Phys Rev B 53:15815
53. Skaff H, Sill K, Emrick T (2004) J Am Chem Soc 126:11322
54. Ginger DS, Greenham NC (1999) Synth Met 101:425
55. Liu P, Su Z (2005) Mater Chem Phys 94:412
56. Rong Y, Hong-Zheng Chen, Wu G, Wang M (2005) Mater Chem Phys 91:370
57. Sharma H, Sharma SN, Singh G, Shivaprasad SM (2005) Proceedings of XIII international workshop on physics of semiconductor devices, vol. I. IWPSD-2005 workshop, NPL India, 13–17 Dec 2005, p 389
58. Cordero SR, Carson PJ, Estabrook RA, Strouse GF, Buratto SK (2000) J Phys Chem B 104:12137
59. Bol AA, Meijerink A (2001) J Phys Chem B 105:10203